# Numerical simulation of tsunami propagation and inundation in East China Sea

Master’s Thesis

# NUMERICAL SIMULATION OF TSUNAMI PROPAGATION AND INUNDATION IN EAST CHINA SEA

March 2017

Graduate School of Marine Science and Technology

Tokyo University of Marine Science and Technology

Master’s Course of Marine System Engineering

CHEN TIANNING

# Contents

## Abstract

After witnessed the destructive power and catastrophic aftermath of 2004 Indian Ocean Tsunami, China started to investigate potential tsunami threat to the Chinese coast. Consequently, the Chinese East China Sea area, the most economically developed and densely populated zone in China, is not an exception of bearing tsunami hazards. Development of a tsunami hazard mitigation solution for the region is a must. However, study about tsunami inundation along coasts facing East China Sea (ECS) has not been carried out yet.

For the reason above, this study aims to fill in the gap by performing numerical simulations of tsunami propagation and inundation in ECS, regarding the difficulties in conducting laboratory experiments that require generation of a tsunami wave in a scale down ECS topography model. The objective of this study is to find the worst tsunami scenario for the Chinese East China Sea coast, and based on this scenario, an inundation map is made for cities which need to be aware of tsunami hazards.

This study only considers tsunamis generated by earthquakes. Earthquakes generated in Ryukyu trench and Okinawa trough are both have possibilities to trigger tsunamis affecting the Chinese coast. To determine the worst tsunami scenario, based on geomorphology, tectonics, seismic activities and historical tsunami records in ECS, two Mw8.2 earthquakes in Okinawa trough and two Mw9.2 earthquakes in Ryukyu trench are selected. The four earthquakes are divided into two categories: North and South. They are set in Tokara strait and Miyako strait respectively. The North cases are used to assess tsunami hazards for areas around Shanghai while the South cases are for study on hazards in Zhejiang Province.

Tsunami wave in ECS has the characteristics of strong nonlinearity and weak dispersion effect, hence nonlinear shallow water equations are chosen as the governing equations. A staggered leap-frog scheme is used to solve the governing equations numerically for its time sufficiency and convenience in dealing with sea boundary conditions. For land boundary, a staircase approximation is applied with adequate accuracy. Since tsunami wave length decreases largely as it propagates into very shallow water, a nested grid system is needed to meet stability of the numerical calculation. Additionally, the calculation should also take bottom friction effect into

account.

A historical tsunami, 1707 Hoei tsunami which affected the Chinese coast, is used to validate the numerical model used in this study. The calculation results are in accordance with previous numerical studies and records in Chinese literatures. Nevertheless, the results vary with bottom roughness. ECS has the feature of water depth lower than 200m in its most parts. The bottom friction effect should be more specifically studied for ECS.

Four hypothetical cases are conducted after model validation. By comparing tsunami height along the Chinese coast of each event, South Ryukyu trench case is spotted as the worst tsunami scenario. The maximum tsunami height along Zhejiang province is about 5m, much higher than that showed in previous studies which was about 2-3m. The inundation distance is up to about 800m. South Taizhou, Dongtou district of Wenzhou, Dachen island can be highly inundated. Their population is over 1 million, 100 thousand, 1 thousand respectively. Without any protection like seawall, it will easily cause hundreds of life casualties and huge economic loss.

More rigorous study about tsunami run-up should be carried out in the future study. In addition, incorporation of high resolution data of bathymetry and topography into the numerical model will also be needed for a solid foundation for tsunami hazard mitigation plans of coastal cities.

# 1. Introduction

## 1.1 Tsunami history

After 2004, we have experienced 13 tsunami events globally. Or in average, not as rare as people usual expected, a tsunami occurred annually. Among these events, 2004 India Ocean tsunami triggered by earthquake of moment magnitude of 9.1-9.3, killed over 230,000 people, making it one of the deadliest natural disasters in human history. Another significant tsunami is 2011 Tohoku tsunami, also induced by earthquake of moment magnitude over 9.0, the highest run-up height was over 40m. It caused over 15,000 life casualties and a nuclear meltdown. The economic loss estimated by World Bank was 235 billion US dollars, let it be the costliest natural disaster in world history. The most recent tsunami event is the one happened in New Zealand on November 14, 2016, just a few months before.

According to Chinese literatures [Wang et al. (2005), Chen et al. (2007), Ren et al. (2014).], there are more than 25 tsunami records along the Chinese coast throughout last 2000 years of Chinese history, as we can see it from Table 1.1 and Figure 1.1.

Table 1.1 Chinese tsunami catalogue

| No. | Time | Longitude | Latitude | Mw |
|---|---|---|---|---|
| 1 | 47BC | 120.0°E | 38.0°N | |
| 2 | 173/7 | 120.4°E | 38.4°N | 7.5 |
| 3 | 1046/4/24 | 121.5°E | 36.5°N | 5.5 |
| 4 | 1076/11 | 117.0°E | 23.0°N | |
| 5 | 1498/7/9 | 131.8°E | 34.0°N | 8.3 |
| 6 | 1509/6 | 121.0°E | 31.5°N | |
| 7 | 1548/9/12 | 121.0°E | 38.0°N | 7 |
| 8 | 1597/10/6 | 120.0°E | 38.5°N | 7 |
| 9 | 1604/12/28 | 119.0°E | 24.7°N | 7.5 |
| 10 | 1605/7/13 | 110.5°E | 20.0°N | 7.5 |
| 11 | 1640/9 | 116.5°E | 23.5°N | 5.75 |
| 12 | 1661/2/15 | 120.2°E | 23.0°N | 6.5 |
| 13 | 1668/7/25 | 118.5°E | 34.8°N | 8.5 |
| 14 | 1670/8/19 | 122.5°E | 33.0°N | 6.75 |
| 15 | 1707/10/28 | 135.9°E | 33.2°N | 8.4 |
| 16 | 1721/9-10 | 120.2°E | 23.0°N | 6 |

| | | | | |
|---|---|---|---|---|
| 17 | 1781/4 | 121.0°E | 24.0°N | 7 |
| 18 | 1792/8/9 | 120.6°E | 23.6°N | 7 |
| 19 | 1854/12/24 | 135.6°E | 33.2°N | 8.4 |
| 20 | 1867/12/18 | 121.8°E | 25.3°N | 7 |
| 21 | 1917/1/25 | 119.4°E | 24.5°N | 6.5 |
| 22 | 1917/7/4 | 123.0°E | 25.0°N | 7.3 |
| 23 | 1918/2/13 | 117.3°E | 23.6°N | 7.3 |
| 24 | 1923/7/13 | 130.5°E | 31.0°N | 7.2 |
| 25 | 1948/5/23 | 121.9°E | 37.6°N | 6 |
| 26 | 1986/11/1 | 121.7°E | 24.1°N | 7.6 |
| 27 | 1994/9/16 | 118.5°E | 23°N | 7.3 |

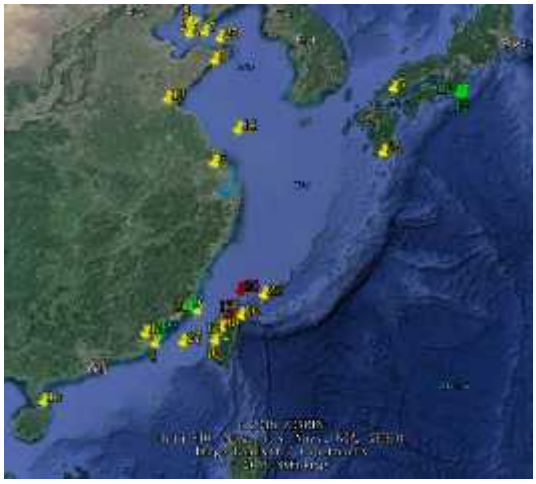

Figure 1.1 Epicenters of Chinese historical tsunami

Although some of these may be documented incorrectly because of people could not distinguish the difference of tsunami and storm surges in ancient time. Nevertheless, most events are confirmed, for mainland China, 1707 Hoei tsunami and 1854 Ansei tsunami which was triggered in Japan Nankai trough has impact to the Chinese East China Sea coast, especially Zhejiang Province and Shanghai. In the case of South China Sea, tsunamis induced by magnitude ≥ 7.0 earthquakes on 1604 and 1918 affected Quanzhou, Fujian Province and Nanao, Guangdong Province, respectively. For Taiwan island, the most devastating tsunami is the one occurred on 1781. It killed more than 40 thousand people in Taiwan. And on 1867, the only instance in China, earthquake and undersea volcano eruption occurred at the same time, the tsunami they generated drown hundreds of people, wrecked countless ships.

Hatori(1988) investigated tsunamis generated from Okinawa trough and Ryukyu trench, indicating that it is an earthquake high-incidence region. The epicenters are showed in Figure 1.2.

Figure 1.2 Tsunami records in Ryukyu region

These tsunamis caused severe damage in Japan, especially 1771 Great Yaeyama tsunami, killed over 13,000 people. The run-up height on Ishigaki island was over 30m. Due to low earthquake magnitude and long distance to the Chinese coast, there are no records in Chinese literatures, but Ryukyu region deserves our high attention when we consider tsunami threat to the Chinese coast.

## 1.2 East China Sea

East China Sea locate at northwest of Pacific Ocean, extend from 21°54′N, 117°05′E to 33°17′N, 131°03′E, about 1300 km in length and 740 km in width, covering an area of approximately 770,000$km^2$ with 370 m

average water depth. It mainly consists of two parts: the continent shelf and Okinawa trough.

The continent shelf is very abroad, occupies about 2/3 area of East China Sea. Generally, it is wider in north than it in south and the longest distance reaches 560 km. Its slope is very mild which between 1/100,000 – 1/1000. And water depth contour is almost in parallel with the Chinese coast. Then shelf break at 160 m water depth. After that is the continent slope zone with 35 km average width. Its slope ranges from 1% to 25%. Earthquake records are rare in the continent shelf region

Okinawa trough, together with Ryukyu island-chain and Ryukyu trench, is a typical trench-arc-back-arc system, induced by Philippine Sea plate subducting Eurasian plate with a rate of 5-7cm/yr. [Wang (2014)]. It is a high earthquake risk region. The mechanism of most earthquake events in Okinawa trough is normal fault or landslide [Liu (2012)] while the common mechanism of earthquake events in Ryukyu trench is reverse fault. Li (2006) analyzed earthquake risks based on the repeatability and analogy of seismic activities in Okinawa trough and Ryukyu trench-arc. He divided Okinawa trough into three potential earthquake regions with magnitude up

limit of 8.0: North, Middle and South. Similar division also was done for Ryukyu trench with exception of maximum magnitude changed to 8.5. However, the two principles used in his analysis are developed from researches of tectonics and seismic activities in plate, it has doubts in its applicability for island region. Moreover, the remoteness of this region and small number of seismometers enlarge the probability of underestimation of seismic activities and magnitude up limit.

### 1.3 Current study

Only few studies have been conducted for tsunami propagation in East China Sea. Basically, it can be divided into three groups based on source region, that is, Nankai trough, Okinawa trough and Ryukyu trench. They are summarized in Table 1.2.

Table 1.2 Current study of tsunami propagation in East China Sea

| Coast \ Source | | Nankai | | | |
|---|---|---|---|---|---|
| | | Wen et al.(2014) 9.1 | | Mao et al.(2015) 9.1 | |
| Jiangsu | North | 1m | 11hrs | | |
| Shanghai | | 2-3m | 8hrs | | |
| Zhejiang | North | 1-2m | 6hrs | 1m+ | 8hrs |
| | Middle | | | 2m+ | 6hrs |
| | South | | | 1m+ | 5hrs |
| Fujian | North | | | | |
| Guangdong | North | | | | |

a. Nankai trough

| Coast \ Source | | Okinawa | | | |
|---|---|---|---|---|---|
| | | Mao et al.(2015) 8.0 | | Liu et al.(2012) 7.0 7.5 8.0 | |
| Jiangsu<br>Shanghai | North | | | | |
| Zhejiang | North | 0.5-1m | 5hrs | 1-2m | 4hrs |
| | Middle | 1-3m | 5hrs | | |
| | South | | 3hrs | | |
| Fujian | North | | | | |
| Guangdong | North | | | | |

b. Okinawa trough

| Coast \ Source | | Ryukyu | | | | | |
|---|---|---|---|---|---|---|---|
| | | Mao et al.(2015) 8.7 | | Lin(2012) 8.8 | | Wen et al.(2016) 9.0 | |
| Jiangsu | North | | | | | | |
| Shanghai | | | | | | 1m | 8hrs |
| Zhejiang | North | 1m | 5hrs | | | 2m | 5hrs |
| | Middle | 1.2-2m | 5hrs | | | | |
| | South | | 3hrs | | | 1-2m | 3-4hrs |
| Fujian | North | | | 2m | 4.5hrs | | |
| Guangdong | North | | | | | 0.5m | 5hrs |

c. Ryukyu trench

Basically, the maximum tsunami height along the Chinese coast is 2-3m, and no study talk about tsunami inundation has been published yet.

## 1.4 Research Objectives

Since previous studies never do tsunami inundation in East China Sea and usually study for one source region only. This study aims to study potential tsunamis in all of three source regions. Determine the worst tsunami scenario by compare their tsunami heights along the Chinese coast. Then use the worst tsunami scenario to obtain inundation map for city planning of seawall construction and others.

## 2. Governing equations and numerical scheme

### 2.1 Governing equations

Tsunami is extreme long wave with wave length of tens to hundreds of kilometers. Water depth of the continent shelf, most part of East China Sea, is less than 160m. For Okinawa trough, the less part, water depth varies from 1000 to 2300m. Average water depth of East China Sea is about 370m. The ratio of water depth to wavelength is less than 1/100, clearly smaller than the up limit of shallow water definition 1/20. Thus, we can consider tsunami in East China Sea as longwave or shallow water wave with strong nonlinearity, also confirmed by Liu et al. (2009). Furthermore, we use a parameter δ proposed by Mei (1989) to determine the importance of dispersion effect. The parameter is defined as

$$\delta = \left(\frac{l}{h}\right)^{\frac{1}{3}}\left(\frac{h}{w}\right) \tag{2.1}$$

where $l$ stands for distance from source region to the leading wave, h and w are water depth and width of fault, respectively. In this case, it is obvious that δ is smaller than one which means dispersion effect is not significant in East China Sea. Also, Ren et al. (2015) suggest that

dispersion effect is neglectable in South China Sea. By using the parameter δ above, we can get the result that dispersion effect is smaller in East China Sea than it in South China Sea. Without high-order derivative terms, as contained in Boussinesque-type equations or Navier-Stokes equation, simulation model will be more efficient.

It can be concluded that it is adequate to use nonlinear shallow water equation as governing equations in East China Sea for tsunami propagation and inundation.

### 2.1.1 Nonlinear shallow water equations

In this study, nonlinear shallow water equations are used in its conservative form. In Cartesian coordinates, they are expressed as

$$\frac{\partial \eta}{\partial t} + \frac{\partial M}{\partial x} + \frac{\partial N}{\partial y} = 0 \tag{2.2}$$

$$\frac{\partial M}{\partial t} + \frac{\partial}{\partial x}\left\{\frac{M^2}{D}\right\} + \frac{\partial}{\partial y}\left\{\frac{MN}{D}\right\} + gD\frac{\partial \eta}{\partial x} + \tau_x = 0 \tag{2.3}$$

$$\frac{\partial N}{\partial t} + \frac{\partial}{\partial x}\left\{\frac{MN}{D}\right\} + \frac{\partial}{\partial y}\left\{\frac{N^2}{D}\right\} + gD\frac{\partial \eta}{\partial y} + \tau_y = 0 \tag{2.4}$$

Where t stands for time, x and y are horizontal coordinates, $\eta$ is water surface elevation, D represents total water depth, M and N are discharge

fluxes (products of depth averaged velocities and total water depth), g is the gravitational acceleration. And bottom friction terms $\tau_x$ and $\tau_y$ are evaluated via Manning's formula

$$\tau_x = \frac{gn^2}{D^{\frac{7}{3}}} M(M^2 + N^2)^{\frac{1}{2}} \tag{2.5}$$

$$\tau_y = \frac{gn^2}{D^{\frac{7}{3}}} N(M^2 + N^2)^{\frac{1}{2}} \tag{2.6}$$

in which n is the Manning's roughness coefficient.

In spherical coordinates, nonlinear shallow water equations are expressed as

$$\frac{\partial \eta}{\partial t} + \frac{1}{R\cos\varphi}\left\{\frac{\partial M}{\partial \psi} + \frac{\partial}{\partial \varphi}(\cos\varphi N)\right\} = 0 \tag{2.7}$$

$$\frac{\partial M}{\partial t} + \frac{1}{R\cos\varphi}\frac{\partial}{\partial \psi}\left\{\frac{M^2}{D}\right\} + \frac{1}{R}\frac{\partial}{\partial \varphi}\left\{\frac{MN}{D}\right\} + \frac{gD}{R\cos\varphi}\frac{\partial \eta}{\partial \psi} + \tau_x = 0 \tag{2.8}$$

$$\frac{\partial N}{\partial t} + \frac{1}{R\cos\varphi}\frac{\partial}{\partial \psi}\left\{\frac{MN}{D}\right\} + \frac{1}{R}\frac{\partial}{\partial \varphi}\left\{\frac{N^2}{D}\right\} + \frac{gD}{R}\frac{\partial \eta}{\partial \psi} + \tau_y = 0 \tag{2.9}$$

Where $\varphi$ and $\psi$ are the latitude and longitude of the Earth, R is the radius of the Earth.

## 2.2 Numerical scheme

We can implement different numerical schemes into nonlinear shallow water equation. Take some existing models for example, TUNAMI model, COMCOT model and MOST model use finite difference scheme whereas

GeoClaw model uses finite volume scheme. And finite element method and other numerical methods are also applicable. This study chooses COMCOT model to conduct numerical studies. Liu et al. (1995) and Wang and Liu. (2006) use it to study 1960 Chile tsunami and 2004 Indian Ocean tsunami respectively, the simulation results are satisfied.

### 2.2.1 Leap-frog scheme

COMCOT model which developed by Cornell University uses an explicit staggered leap-frog finite difference scheme. More specifically, central difference scheme for linear terms and upwind scheme for nonlinear terms. Because if we applied central difference scheme to nonlinear terms, it will introduce a negative diffusion error which leads to instability. So, the accuracy of numerical calculation goes down to $1^{st}$ order if we include nonlinear terms. Arrangement of computation points are shown in Figure 2.1 a and b. $\eta$ is set at the center of a computation cell, it has half computation step difference from discharge flux M and N in both time and space. This special arrangement eases boundary conditions setting.

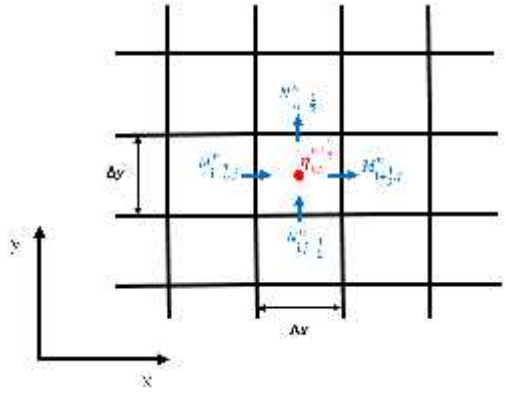

a

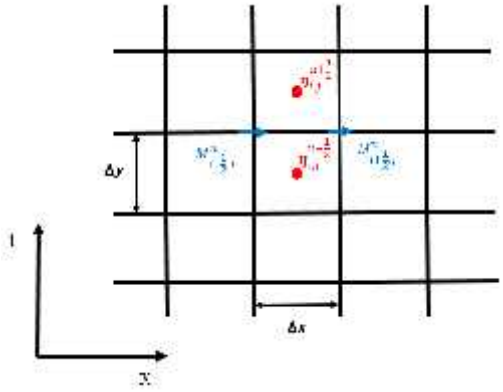

b

Figure 2.1 Arrangement of computation grids

Therefore, discretized equations use central difference scheme for linear terms in Cartesian coordinates is given as

$$\frac{\eta_{i,j}^{n+\frac{1}{2}}-\eta_{i,j}^{n-\frac{1}{2}}}{\Delta t}+\frac{M_{i+\frac{1}{2},j}^{n}-M_{i-\frac{1}{2},j}^{n}}{\Delta x}+\frac{N_{i,j+\frac{1}{2}}^{n}-N_{i,j-\frac{1}{2}}^{n}}{\Delta y}=0 \qquad (2.10)$$

$$\frac{M_{i+\frac{1}{2},j}^{n+1}-M_{i+\frac{1}{2},j}^{n}}{\Delta t}+gD_{i+\frac{1}{2},j}^{n+\frac{1}{2}}\frac{\eta_{i+1,j}^{n+\frac{1}{2}}-\eta_{i,j}^{n+\frac{1}{2}}}{\Delta x}=0 \qquad (2.11)$$

$$\frac{N^{n+1}_{i,j+\frac{1}{2}}-N^{n}_{i,j+\frac{1}{2}}}{\Delta t}+\mathrm{gD}^{n+\frac{1}{2}}_{i,j+\frac{1}{2}}\frac{\eta^{n+\frac{1}{2}}_{i,j+1}-\eta^{n+\frac{1}{2}}_{i,j}}{\Delta y}=0 \tag{2.12}$$

and its counterpart in spherical coordinates are expressed as

$$\frac{\eta^{n+\frac{1}{2}}_{i,j}-\eta^{n-\frac{1}{2}}_{i,j}}{\Delta t}+\left\{\frac{1}{R\cos\varphi}\right\}_{i,j}\frac{M^{n}_{i+\frac{1}{2},j}-M^{n}_{i-\frac{1}{2},j}}{\Delta\psi}+$$

$$\left\{\frac{1}{R\cos\varphi}\right\}_{i,j}\frac{\left(\cos\varphi_{i,j+\frac{1}{2}}\right)N^{n}_{i,j+\frac{1}{2}}-\left(\cos\varphi_{i,j-\frac{1}{2}}\right)N^{n}_{i,j-\frac{1}{2}}}{\Delta\varphi}=0 \tag{2.13}$$

$$\frac{M^{n+1}_{i+\frac{1}{2},j}-M^{n}_{i+\frac{1}{2},j}}{\Delta t}+\frac{\mathrm{gD}^{n+\frac{1}{2}}_{i+\frac{1}{2},j}}{R\cos\varphi_{i+\frac{1}{2},j}}\frac{\eta^{n+\frac{1}{2}}_{i+1,j}-\eta^{n+\frac{1}{2}}_{i,j}}{\Delta\psi}=0 \tag{2.14}$$

$$\frac{N^{n+1}_{i,j+\frac{1}{2}}-N^{n}_{i,j+\frac{1}{2}}}{\Delta t}+\frac{\mathrm{gD}^{n+\frac{1}{2}}_{i,j+\frac{1}{2}}}{R}\frac{\eta^{n+\frac{1}{2}}_{i,j+1}-\eta^{n+\frac{1}{2}}_{i,j}}{\Delta\varphi}=0 \tag{2.15}$$

Since we use upwind scheme for nonlinear terms in the momentum equations, in Cartesian coordinates they are discretized as

$$\frac{\partial}{\partial x}\left\{\frac{M^2}{D}\right\}=\frac{1}{\Delta x}\left\{\lambda_{11}\frac{\left(M^{n}_{i+\frac{3}{2},j}\right)^2}{D^{n}_{i+\frac{3}{2},j}}+\lambda_{12}\frac{\left(M^{n}_{i+\frac{1}{2},j}\right)^2}{D^{n}_{i+\frac{1}{2},j}}+\lambda_{13}\frac{\left(M^{n}_{i-\frac{1}{2},j}\right)^2}{D^{n}_{i-\frac{1}{2},j}}\right\} \tag{2.16}$$

$$\frac{\partial}{\partial y}\left\{\frac{MN}{D}\right\}=\frac{1}{\Delta y}\left\{\lambda_{21}\frac{(MN)^{n}_{i+\frac{1}{2},j+1}}{D^{n}_{i+\frac{1}{2},j+1}}+\lambda_{22}\frac{(MN)^{n}_{i+\frac{1}{2},j}}{D^{n}_{i+\frac{1}{2},j}}+\lambda_{23}\frac{(MN)^{n}_{i+\frac{1}{2},j-1}}{D^{n}_{i+\frac{1}{2},j-1}}\right\} \tag{2.17}$$

$$\frac{\partial}{\partial x}\left\{\frac{MN}{D}\right\}=\frac{1}{\Delta x}\left\{\lambda_{31}\frac{(MN)^{n}_{i+1,j+\frac{1}{2}}}{D^{n}_{i+1,j+\frac{1}{2}}}+\lambda_{32}\frac{(MN)^{n}_{i,j+\frac{1}{2}}}{D^{n}_{i,j+\frac{1}{2}}}+\lambda_{33}\frac{(MN)^{n}_{i-1,j+\frac{1}{2}}}{D^{n}_{i-1,j+\frac{1}{2}}}\right\} \tag{2.18}$$

$$\frac{\partial}{\partial y}\left\{\frac{M^2}{D}\right\}=\frac{1}{\Delta y}\left\{\lambda_{41}\frac{\left(M^{n}_{i,j+\frac{3}{2}}\right)^2}{D^{n}_{i,j+\frac{3}{2}}}+\lambda_{42}\frac{\left(M^{n}_{i,j+\frac{1}{2}}\right)^2}{D^{n}_{i,j+\frac{1}{2}}}+\lambda_{43}\frac{\left(M^{n}_{i,j-\frac{1}{2}}\right)^2}{D^{n}_{i,j-\frac{1}{2}}}\right\} \tag{2.19}$$

Where $\boldsymbol{\lambda}$, depend on flow direction, are determined from

$$\begin{cases} \lambda_{11}=0, & \lambda_{12}=1, & \lambda_{13}=-1, & if M^{n}_{i+\frac{1}{2},j} \geq 0 \\ \lambda_{11}=1, & \lambda_{12}=-1, & \lambda_{13}=0, & if M^{n}_{i+\frac{1}{2},j} < 0 \end{cases} \tag{2.20}$$

$$\begin{cases} \lambda_{21}=0, & \lambda_{22}=1, & \lambda_{23}=-1, & if N^{n}_{i+\frac{1}{2},j} \geq 0 \\ \lambda_{21}=1, & \lambda_{22}=-1, & \lambda_{23}=0, & if N^{n}_{i+\frac{1}{2},j} < 0 \end{cases} \tag{2.21}$$

$$\begin{cases} \lambda_{31}=0, & \lambda_{32}=1, & \lambda_{33}=-1, & if M^{n}_{i,j+\frac{1}{2}} \geq 0 \\ \lambda_{31}=1, & \lambda_{32}=-1, & \lambda_{33}=0, & if M^{n}_{i,j+\frac{1}{2}} < 0 \end{cases} \tag{2.22}$$

$$\begin{cases} \lambda_{41}=0, & \lambda_{42}=1, & \lambda_{43}=-1, & if N^{n}_{i,j+\frac{1}{2}} \geq 0 \\ \lambda_{41}=1, & \lambda_{42}=-1, & \lambda_{43}=0, & if N^{n}_{i,j+\frac{1}{2}} < 0 \end{cases} \tag{2.23}$$

Additionally, the bottom frictional terms are discretized as

$$F_x = v_x\left(M^{n+1}_{i+\frac{1}{2},j} + M^{n}_{i+\frac{1}{2},j}\right) \tag{2.24}$$

$$F_y = v_y\left(N^{n+1}_{i,j+\frac{1}{2}} + N^{n}_{i,j+\frac{1}{2}}\right) \tag{2.25}$$

Where $v_x$ and $v_y$ are given as

$$v_x = \frac{1}{2}\frac{gn^2}{\left(D^{n}_{i+\frac{1}{2},j}\right)^{\frac{7}{3}}}\left[\left(M^{n}_{i+\frac{1}{2},j}\right)^2 + \left(N^{n}_{i+\frac{1}{2},j}\right)^2\right]^{\frac{1}{2}} \tag{2.26}$$

$$v_y = \frac{1}{2}\frac{gn^2}{\left(D^{n}_{i,j+\frac{1}{2}}\right)^{\frac{7}{3}}}\left[\left(M^{n}_{i,j+\frac{1}{2}}\right)^2 + \left(N^{n}_{i,j+\frac{1}{2}}\right)^2\right]^{\frac{1}{2}} \tag{2.27}$$

At last, solutions of discretized equations are given as

$$\eta^{n+\frac{1}{2}}_{i,j} = \eta^{n-\frac{1}{2}}_{i,j} - r_x\left(M^{n}_{i+\frac{1}{2},j} - M^{n}_{i-\frac{1}{2},j}\right) + r_y\left(N^{n}_{i,j+\frac{1}{2}} - N^{n}_{i,j-\frac{1}{2}}\right) \tag{2.28}$$

$$M^{n+1}_{i+\frac{1}{2},j} = \frac{1}{1+v_x\Delta t}\left\{(1-v_x\Delta t)M^{n}_{i+\frac{1}{2},j} - r_x \mathrm{g} \mathrm{D}^{n+\frac{1}{2}}_{i+\frac{1}{2},j}\left(\eta^{n+\frac{1}{2}}_{i+1,j} - \eta^{n+\frac{1}{2}}_{i,j}\right)\right\} -$$

$$\frac{r_x}{1+v_x\Delta t}\left\{\lambda_{11}\frac{\left(M^n_{i+\frac{3}{2},j}\right)^2}{D^n_{i+\frac{3}{2},j}}+\lambda_{12}\frac{\left(M^n_{i+\frac{1}{2},j}\right)^2}{D^n_{i+\frac{1}{2},j}}+\lambda_{13}\frac{\left(M^n_{i-\frac{1}{2},j}\right)^2}{D^n_{i-\frac{1}{2},j}}\right\}-$$

$$\frac{r_x}{1+v_x\Delta t}\left\{\lambda_{21}\frac{(MN)^n_{i+\frac{1}{2},j+1}}{D^n_{i+\frac{1}{2},j+1}}+\lambda_{22}\frac{(MN)^n_{i+\frac{1}{2},j}}{D^n_{i+\frac{1}{2},j}}+\lambda_{23}\frac{(MN)^n_{i+\frac{1}{2},j-1}}{D^n_{i+\frac{1}{2},j-1}}\right\} \quad (2.29)$$

$$N^{n+1}_{i,j+\frac{1}{2}}=\frac{1}{1+v_y\Delta t}\left\{(1-v_y\Delta t)N^n_{i,j+\frac{1}{2}}-r_y\mathrm{g}D^{n+\frac{1}{2}}_{i,j+\frac{1}{2}}\left(\eta^{n+\frac{1}{2}}_{i,j+1}-\eta^{n+\frac{1}{2}}_{i,j}\right)\right\}-$$

$$\frac{r_y}{1+v_y\Delta t}\left\{\lambda_{31}\frac{(MN)^n_{i+1,j+\frac{1}{2}}}{D^n_{i+1,j+\frac{1}{2}}}+\lambda_{32}\frac{(MN)^n_{i,j+\frac{1}{2}}}{D^n_{i,j+\frac{1}{2}}}+\lambda_{33}\frac{(MN)^n_{i-1,j+\frac{1}{2}}}{D^n_{i-1,j+\frac{1}{2}}}\right\}-$$

$$\frac{r_y}{1+v_y\Delta t}\left\{\lambda_{41}\frac{\left(M^n_{i,j+\frac{3}{2}}\right)^2}{D^n_{i,j+\frac{3}{2}}}+\lambda_{42}\frac{\left(M^n_{i,j+\frac{1}{2}}\right)^2}{D^n_{i,j+\frac{1}{2}}}+\lambda_{43}\frac{\left(M^n_{i,j-\frac{1}{2}}\right)^2}{D^n_{i,j-\frac{1}{2}}}\right\} \quad (2.30)$$

Where $r_x=\Delta t/\Delta x$ and $r_y=\Delta t/\Delta y$. Some simple approximations are also used in the above equations:

$$D^{n+\frac{1}{2}}_{i+\frac{1}{2},j}=\frac{1}{2}\left(D^{n+\frac{1}{2}}_{i,j}+D^{n+\frac{1}{2}}_{i+1,j}\right) \quad (2.31)$$

$$D^{n+\frac{1}{2}}_{i,j+\frac{1}{2}}=\frac{1}{2}\left(D^{n+\frac{1}{2}}_{i,j}+D^{n+\frac{1}{2}}_{i,j+\frac{1}{2}}\right) \quad (2.32)$$

$$D^{n}_{i+\frac{1}{2},j}=\frac{1}{4}\left(D^{n-\frac{1}{2}}_{i,j}+D^{n+\frac{1}{2}}_{i,j}+D^{n-\frac{1}{2}}_{i+1,j}+D^{n+\frac{1}{2}}_{i+1,j}\right) \quad (2.33)$$

$$D^{n}_{i,j+1/2}=\frac{1}{4}\left(D^{n-\frac{1}{2}}_{i,j}+D^{n+\frac{1}{2}}_{i,j}+D^{n-\frac{1}{2}}_{i,j+1}+D^{n+\frac{1}{2}}_{i,j+1}\right) \quad (2.34)$$

$$M^{n}_{i,j+\frac{1}{2}} = \frac{1}{4}\left(M^{n}_{i-\frac{1}{2},j} + M^{n}_{i-\frac{1}{2},j+1} + M^{n}_{i+\frac{1}{2},j} + M^{n}_{i+\frac{1}{2},j+1}\right) \quad (2.35)$$

$$N^{n}_{i+\frac{1}{2},j} = \frac{1}{4}\left(N^{n}_{i,j-\frac{1}{2}} + N^{n}_{i+1,j-\frac{1}{2}} + N^{n}_{i,j+\frac{1}{2}} + N^{n}_{i+1,j+\frac{1}{2}}\right) \quad (2.36)$$

In spherical coordinates, the solutions are written as

$$\eta^{n+\frac{1}{2}}_{i,j} = \eta^{n-\frac{1}{2}}_{i,j} - \frac{1}{Rcos\varphi_{ij}}\frac{\Delta t}{\Delta\psi}\left(M^{n}_{i+\frac{1}{2},j} - M^{n}_{i-\frac{1}{2},j}\right) - \frac{1}{R}\frac{\Delta t}{\Delta\varphi}\left(N^{n}_{i,j+\frac{1}{2}} - N^{n}_{i,j-\frac{1}{2}}\right) \quad (2.37)$$

$$M^{n+1}_{i+\frac{1}{2},j} = J_x\left\{(1 - v_x\Delta t)M^{n}_{i+\frac{1}{2},j} - \left\{\frac{\mathrm{gD}}{Rcos\varphi}\right\}^{n+\frac{1}{2}}_{i+\frac{1}{2},j}\frac{\Delta t}{\Delta\psi}\left(\eta^{n+\frac{1}{2}}_{i+1,j} - \eta^{n+\frac{1}{2}}_{i,j}\right)\right\} -$$

$$\frac{J_x}{Rcos\varphi_{i,j}}\frac{\Delta t}{\Delta\psi}\left\{\lambda_{11}\frac{\left(M^{n}_{i+\frac{3}{2},j}\right)^2}{D^{n}_{i+\frac{3}{2},j}} + \lambda_{12}\frac{\left(M^{n}_{i+\frac{1}{2},j}\right)^2}{D^{n}_{i+\frac{1}{2},j}} + \lambda_{13}\frac{\left(M^{n}_{i-\frac{1}{2},j}\right)^2}{D^{n}_{i-\frac{1}{2},j}}\right\} -$$

$$\frac{J_x}{R}\frac{\Delta t}{\Delta\varphi}\left\{\lambda_{21}\frac{(MN)^{n}_{i+\frac{1}{2},j+1}}{D^{n}_{i+\frac{1}{2},j+1}} + \lambda_{22}\frac{(MN)^{n}_{i+\frac{1}{2},j}}{D^{n}_{i+\frac{1}{2},j}} + \lambda_{23}\frac{(MN)^{n}_{i+\frac{1}{2},j-1}}{D^{n}_{i+\frac{1}{2},j-1}}\right\} \quad (2.38)$$

$$N^{n+1}_{i,j+\frac{1}{2}} = J_y\left\{\left(1 - v_y\Delta t\right)M^{n}_{i,j+\frac{1}{2}} - \frac{\mathrm{gD}^{n+\frac{1}{2}}_{i,j+\frac{1}{2}}}{R}\frac{\Delta t}{\Delta\varphi}\left(\eta^{n+\frac{1}{2}}_{i,j+1} - \eta^{n+\frac{1}{2}}_{i,j}\right)\right\} -$$

$$\frac{J_y}{Rcos\varphi_{i,j+\frac{1}{2}}}\frac{\Delta t}{\Delta\psi}\left\{\lambda_{31}\frac{(MN)^{n}_{i+1,j+\frac{1}{2}}}{D^{n}_{i+1,j+\frac{1}{2}}} + \lambda_{32}\frac{(MN)^{n}_{i,j+\frac{1}{2}}}{D^{n}_{i,j+\frac{1}{2}}} + \lambda_{33}\frac{(MN)^{n}_{i-1,j+\frac{1}{2}}}{D^{n}_{i-1,j+\frac{1}{2}}}\right\} -$$

$$\frac{J_y}{R}\frac{\Delta t}{\Delta\varphi}\left\{\lambda_{41}\frac{\left(M^{n}_{i,j+\frac{3}{2}}\right)^2}{D^{n}_{i,j+\frac{3}{2}}} + \lambda_{42}\frac{\left(M^{n}_{i,j+\frac{1}{2}}\right)^2}{D^{n}_{i,j+\frac{1}{2}}} + \lambda_{43}\frac{\left(M^{n}_{i,j-\frac{1}{2}}\right)^2}{D^{n}_{i,j-\frac{1}{2}}}\right\} \quad (2.39)$$

where $J_x = \frac{1}{1+v_x\Delta t}$ and $J_y = \frac{1}{1+v_y\Delta t}$. And other variables remain same as

they are used in Cartesian coordinates.

### 2.2.2 Nested Grid

As tsunami propagating toward shoreline, water depth decrease gradually as well as tsunami wavelength. In numerical computation, on one hand, at least 20 grids should be covered in one local tsunami wavelength [Shuto et al. (1986)]. On the other hand, we cannot set infinite grids regard of Courant number or stability analysis, otherwise it will take enormous computation time which is unnecessary and unfordable economically. An effective solution is to adopt nested grid system that allows the usage of relatively coarse grid in deep ocean and finer gird in coastal regions. Both time efficiency and calculation accuracy will be quite satisfying if we use nested grid ingeniously.

In COMCOT, computation cells are assumed as squared, or say $\Delta x = \Delta y$. In each grid layer of nested grid system, space step should be uniform. However, time step can be different for different layers, depends on the grid size and maximum water depth of each layer, to satisfy Courant-Friedrichs-Lewy (CFL) condition. Just to illustrate nested grid,

Figure 2.3 gives us a simple two layers of nested grid as an example. Dots represent water surface elevation $\eta$, while arrows denote discharge fluxes M and N. In Figure 2.3, the grid ratio of the outer layer and the inner layer is 1:3, so discharge fluxes in the outer layer are interpolated into the inner layer at the boundary of two layers for further calculation. In fact, we can set any integer ratio to the system, but since there is a “true” value in the middle of the boundary, it prefers to use odd number ratio. Furthermore, regarding of stability and accuracy, ratio of 3 is always recommended.

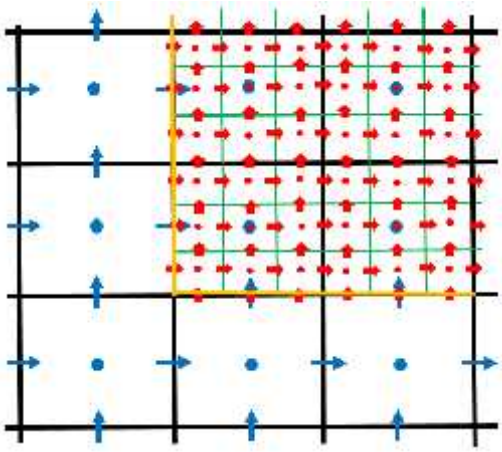

Figure 2.2 Two layers of nested grid

### 2.2.3 Boundary conditions

It is not easy to describe moving boundary (land boundary) by equations in the Eulerian description. In COMCOT, it approximates real bathymetry

and topography by staircase of computation cells and the result is adequate. Take one-dimensional case shown in Figure 2.3 as an example. After getting the latest water surface elevation value from the continuity equation, we can focus on the nearest land cell to determine the position of shoreline. Based on the assumption of $D_i > 0$, the algorithm of determine shoreline is summarized as follows:

If $D_{i+1} \leq 0$ and $h_{i+1} + \eta_i \leq 0$, then the computation cell i+1 is not inundated, the discharge flux $M_{i+\frac{1}{2}}$ keeps have a zero value.

If $D_{i+1} \leq 0$ and $h_{i+1} + \eta_i > 0$, then the computation cell i+1 is inundated, and the discharge flux $M_{i+\frac{1}{2}}$ becomes nonzero. The inundation depth is determined by $H_f = h_{i+1} + \eta_i$.

If $D_{i+1} > 0$, then the computation cell i+1 is inundated, and the discharge flux $M_{i+\frac{1}{2}}$ becomes nonzero. The inundation depth is determined by $H_f = \max(h_{i+1} + \eta_i, h_{i+1} + \eta_{i+1})$.

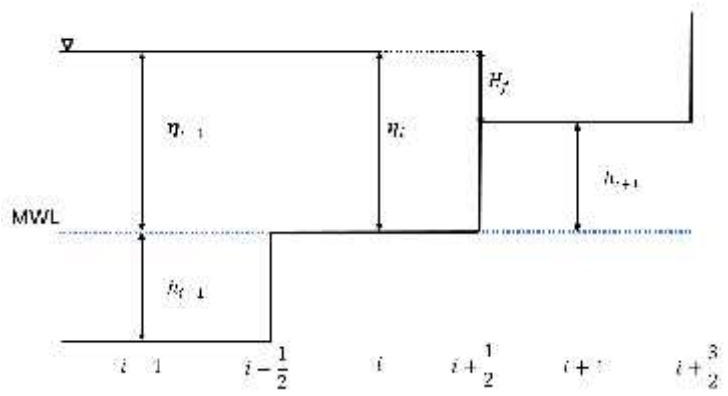


Figure 2.3 Moving boundary scheme

For sea boundary, COMCOT provides three options: open boundary condition, sponge boundary condition and input boundary condition. Open boundary condition is used in this study. It allows water waves to travel outward through the boundaries without any barrier. The centers of boundary computation cells where water surface elevation $\eta$ located are defined as sea boundaries. Therefore, at every time step, $\eta$ at the boundary cells which are not able to be computed need to be given by another way. This is done by using linear shallow water theory as follows

$$\eta = \frac{\sqrt{M^2+N^2}}{\sqrt{gh}} \tag{2.40}$$

where h is the still water depth and $\eta$, M, N and g are defined same as above.

## 3. Numerical experiment

Governing equations used in this study are nonlinear shallow water equations in spherical coordinates. Bathymetry and topography data of all numerical experiments are given by Etopo1 1-min data (available for download at https://maps.ngdc.noaa.gov/viewers/wcs-client/). For inner layers of nested grid, their data are all interpolated from Etopo1 1-min data. The outmost layer of nested grid adopts 1 arc-min bathymetry and topography resolution and the ratio of two adjacent layers is fixed at 3. Computation time step is 1s in all numerical experiments. Without special explanation, tidal level is always zero for initial water level setting. The source model of earthquake induced tsunamis is Okada's model[Okada (1985)]. Bathymetry data of East China Sea is shown in Figure 3.1.

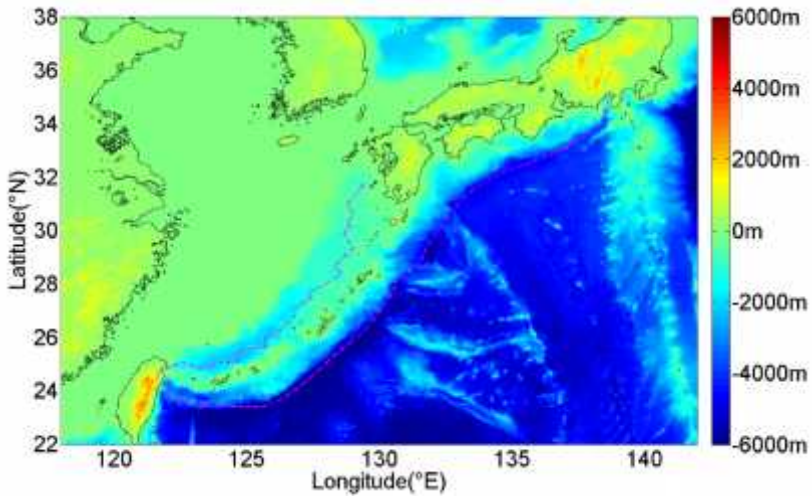


Figure 3.1 Bathymetry of East China Sea

## 3.1 Validation test

### 3.1.1 1707 Hoei tsunami

Same as Ryukyu trench, Nankai trough formed by Philippine Sea plate subducting Eurasian plate. A great earthquake of magnitude 8.4 happened on October 28,1707. This great earthquake was the biggest earthquake in the history of Japan before the 2011 Tohoku earthquake. It caused a destructive tsunami and over 5000 casualties in Japan. Some Chinese documents record that on the same breezeless day the water level rose suddenly and rapidly in Qiantang river and other places of Zhejiang province [Wang et al. (2005)]. In this study, this tsunami event is used for validation test of COMCOT model.

The test adopts two layers of nested grid. Domain of the outer layer is 22°N~38°N, 118°E~142°E. It covers from the Chinese East China Sea coast to the whole Nankai trough. Domain of the inner layer is 27°N~33°N, 119°E~124°E. It focuses on the Chinese coast and its near sea. The nested grid setting and initial wave is shown in Figure 3.2.

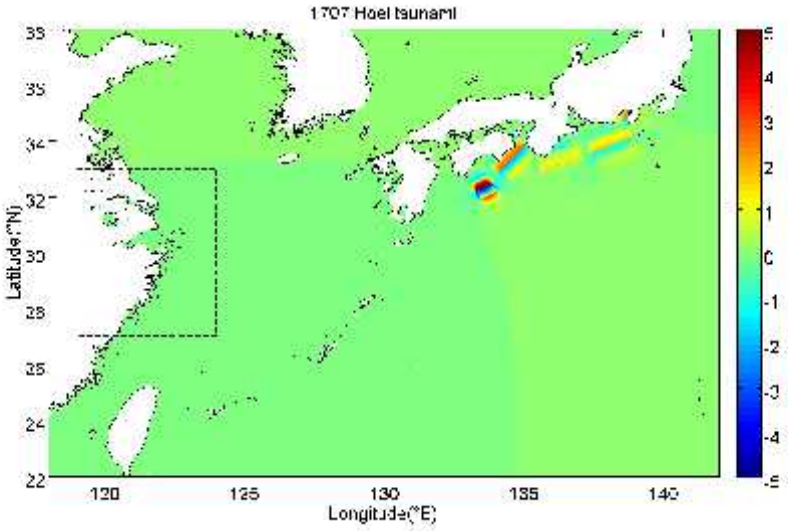


Figure 3.2 Initial wave surface profile of 1707 Hoei tsunami (Aida,1981)

Fault parameters of the earthquake are based on Aida (1981). It divided Nankai trough into five segments as we can see from Table 3.1.

Table 3.1 Fault parameters of 1707 Hoei earthquake(Aida, 1981)

| Location | Depth/(km) | Strike/(°) | Dip/(°) | Slip/(°) | Dislocation/(m) | Length/(km) | Width(km) |
|---|---|---|---|---|---|---|---|
| 33.14°N, 136.73°E | 2 | 193 | 31 | 71 | 4 | 115 | 70 |
| 33.90°N, 136.13°E | 3 | 245 | 24 | 113 | 4 | 150 | 100 |
| 33.41°N, 136.16°E | 10 | 250 | 10 | 124 | 5.6 | 150 | 70 |
| 33.10°N, 134.67°E | 1 | 220 | 20 | 90 | 7 | 140 | 80 |
| 32.33°N, 133.57°E | 1 | 240 | 20 | 90 | 13.9 | 80 | 80 |

Figure 3.3 shows us the maximum tsunami coastal heights along the Chinese coast. The maximum coastal height of the model calculated is in accordance with previous numerical studies' 0.7m (Harada and Satake 2014; Kim et al. 2016).

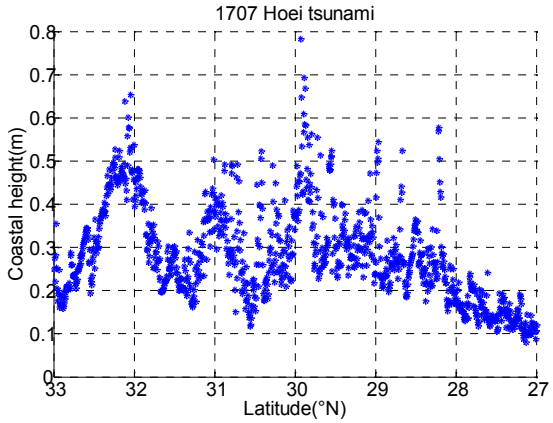


Figure 3.3 Tsunami coastal heights along the Chinese coast

## 3.2 Hypothetical tsunami

### 3.2.1 Interested area and source selection

Most part of Fujian province is protected by Taiwan island from tsunami in East China Sea. Regarding of the purpose of this study, Zhejiang province, Shanghai and Jiangsu province, namely Yangtze river delta region, are the research interesting areas in this study. More specifically, Zhejiang coasts are in the innermost layer of nested grid for tsunami generated in south Okinawa trough and Ryukyu trench while Yangtze river mouth and Hangzhou bay region are the main study area for tsunami generated in north Okinawa trough and Ryukyu trench.

Since the final goal is to determine the worst tsunami scenario,

earthquakes with big magnitude, “good” location and short distance to the Chinese coast are what we are looking for.

Li (2006) set up limit magnitude 8.0 for Okinawa trough and 8.5 for Ryukyu trench. However, his method has uncertainties. To avoid this, Rong et al. (2014) replace maximum earthquake magnitude by add a time period of interest. Most of the circum-Pacific subduction zones will have a magnitude ≥ 9.0 earthquake over a 10,000-year interval. Moreover, Lin et al. (2014) suggest that geodynamic contexts are similar between the Sumatra and Ryukyu subduction zones, a potential magnitude ≥ 9.0 earthquake may occur in the fore-arc area of the Ryukyu subduction zone. Thus, magnitude 8.2 and 9.2 earthquake are set in Okinawa trough and Ryukyu trench, respectively. In terms of epicenter location, Tokara strait and Miyako strait are two candidates for our simulation. This setting is to minimize the function of islands in East China Sea as “natural breakwater”. For earthquakes in Okinawa trough, they are set near the end of the continent shelf since there are few islands in the continent shelf area and the distance between tsunami source to the Chinese coast can be an important factor.

### 3.2.2 Okinawa trough

Earthquake magnitude in Okinawa trough is set as Mw 8.2 and by using a scaling law of Utsu (2001) we can get fault length and width. Because in this source region the major factor of tsunami impacts to the Chinese coast is the distance from source to coast, two experiments marked as ON.n and ON.s (ON stands for Okinawa trough, n means north and s means south), referred from Harvard CMT catalog 1977-1998, are set near the east end of the continent shelf from north to south. Epicenter locations and fault parameters are listed in Table 3.2.

Table 3.2 Fault parameters of two experiments in Okinawa trough

| Case | Location | Depth/(km) | Strike/(°) | Dip/(°) | Slip/(°) | Dislocation/(m) | Length/(km) | Width(km) |
|---|---|---|---|---|---|---|---|---|
| ON.n | 29.20°N, 128.20°E | 10 | 205 | 55 | 90 | 9.2 | 184 | 92 |
| ON.s | 26.20°N, 125.60°E | 10 | 220 | 55 | 90 | 9.2 | 184 | 92 |

The range of three nested grid layers of case ON.n is 21°N~35°N, 118°E~140°E, 27°N~33°N, 119°E~124°E, 28.8°N~32.8°N, 120°E~123.5°E from outmost layer to innermost layer respectively. For case ON.s, the outmost layer narrows down to 21°N~35°N, 118°E~132°E, the second layer is same as case ON.n, and since it generated tsunami from south Okinawa trough, the third layer that focus on Zhejiang coasts ranges from 27.7°N~30.2°N, 120.5°E~123°E. Grid setting and initial wave

profiles of case ON.n and ON.s are shown in Figure 3.4 a and b. the two experiments both ran for 15 hours which assures tsunami waves impact the Chinese coast completely.

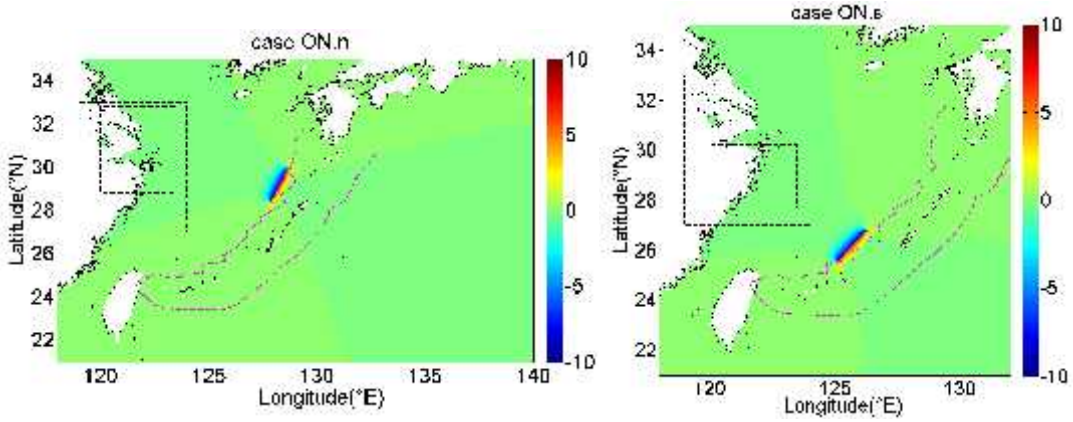


a b

Figure 3.4 Nested grid and initial wave profiles of case ON.a and ON.b. Pink dashed lines represent plate boundary between Eurasian Plate and Philippine Sea Plate (Bird 2003).

After running 15 hours, their maximum wave amplitude distributions are shown in Figure 3.5.

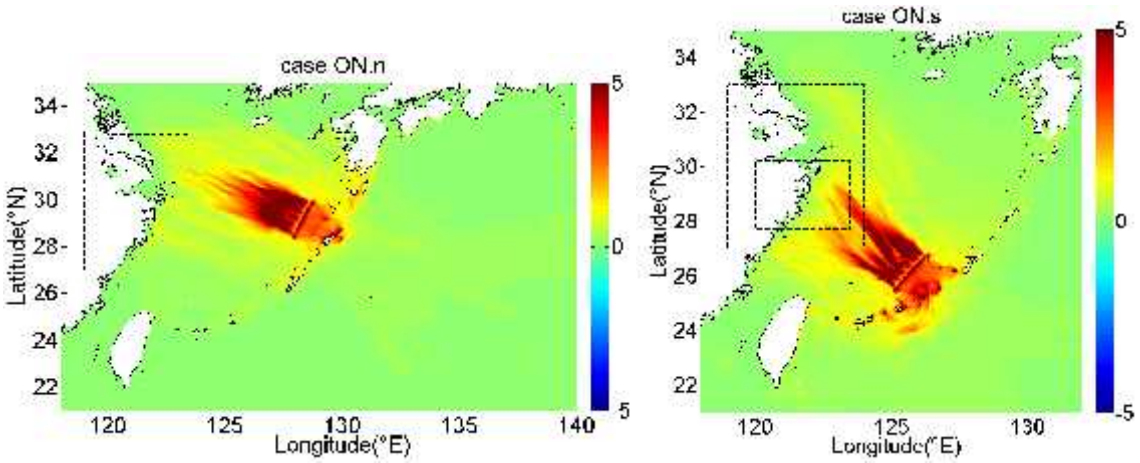


a)ON.n b)ON.s

Figure 3.5 Maximum wave amplitude distributions of ON cases

### 3.2.3 Ryukyu trench

Seismic magnitude of Ryukyu trench is set as Mw 9.2. Same procedure as above, length and width of fault are calculated by using scaling law. Two experiments, RK.a and RK.b (RK stands for Ryukyu trench), are set in Tokara Strait and Miyako Strait respectively. The reason why these two straits are chosen is that among the whole Ryukyu region, the role of islands play as natural breakwater goes down to minimum in the two wide gaps. Additionally, the degree of tsunami wave attenuation varies with tsunami propagating direction [Murata et al. (2009)], so directions of the earthquakes are specially set to maximize tsunami threat to the major cities

along the Chinese coast. Historically, 1911 Kikai Island Earthquake with seismic magnitude of Mw 8.0 happened near case RK.a, and 1771 Yaeyama Great Earthquake probably accompanied with landslide generated close to case RK.b. Table 3.3 shows locations and fault parameters of the two hypothetical events.

Table 3.3 Fault parameters of two numerical experiments in Ryukyu trench

| Case | Location | Depth/(km) | Strike/(°) | Dip/(°) | Slip/(°) | Dislocation/(m) | Length/(km) | Width/(km) |
|---|---|---|---|---|---|---|---|---|
| RK.n | 28.60°N, 130.00°E | 50.5 | 196 | 30 | 90 | 20.7 | 415 | 206 |
| RK.s | 25.10°N, 126.20°E | 50.5 | 217 | 30 | 90 | 20.7 | 427 | 200 |

For nested grid setting, case RK.n and RK.s are as same as case ON.n and On.s, respectively. Their initial wave profiles are shown in Figure 3.6 a and b. The two experiments also ran for 15 hours.

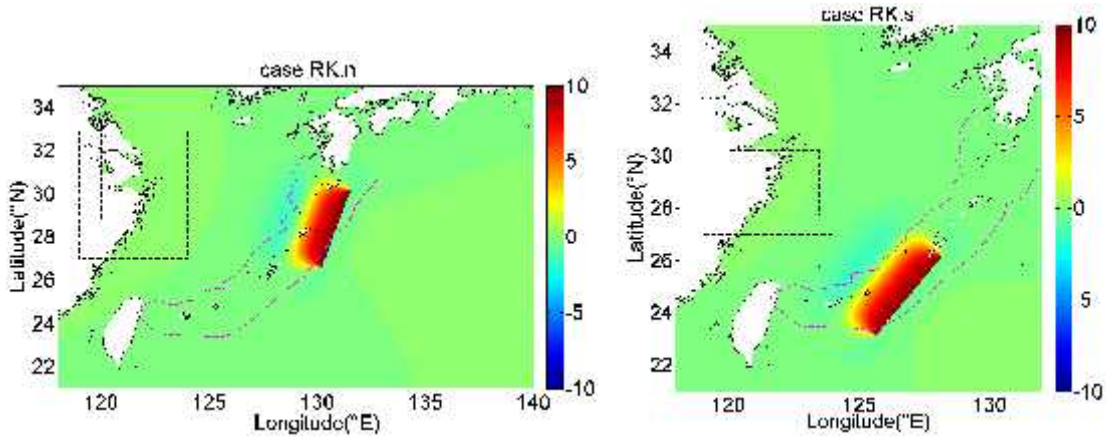


a b

Figure 3.6 Nested grid and initial wave of case RK.n and RK.s.

Figure 3.7 shows maximum wave amplitude distributions of cases in

Ryukyu trench after the model running 15 hours,

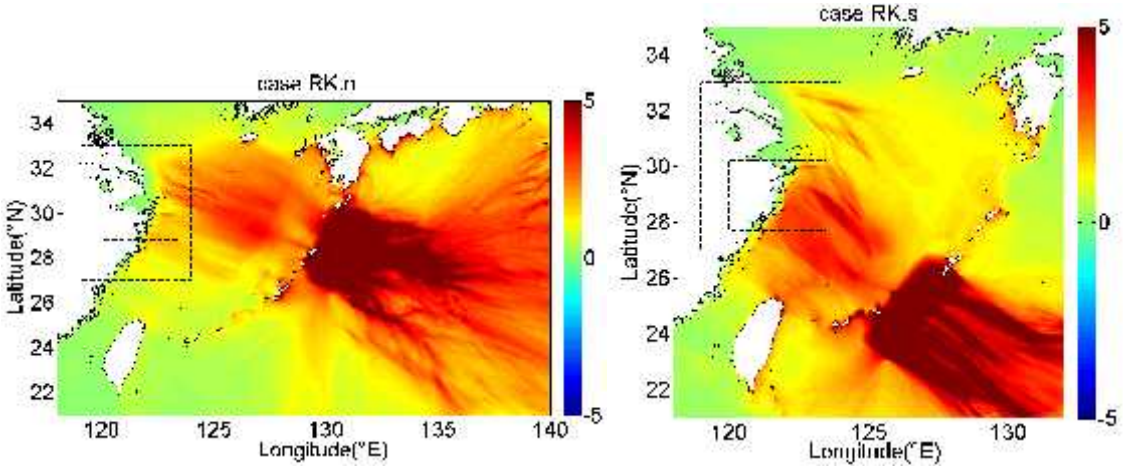


a)RK.n b)RK.s

Figure 3.7 Maximum wave amplitude distributions of RK cases

### 3.3 Comparison

Because the domain of the third layer is different for north and south cases. We compare the maximum tsunami coastal heights separately, that is, north cases are used to study about coasts around Shanghai while south cases are focus on Zhejiang coasts.

#### 3.3.1 Shanghai coasts

We use case ON.n and RK.n to compare the maximum tsunami coastal heights of coasts around Shanghai. The comparison result is shown in Figure 3.8.

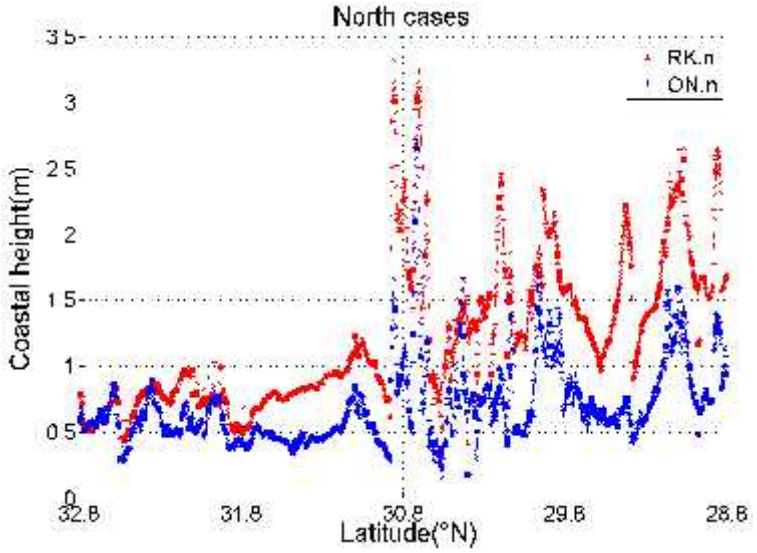


Figure 3.8 The maximum tsunami coastal heights comparison (North cases)

As a result, case RK.n is more threatening than ON.n in the case of the Chinese coast.

### 3.3.2 Zhejiang coasts

Case ON.s and RK.s are used to compare the maximum tsunami coastal heights of Zhejiang coasts. The comparison result is shown in Figure 3.9.

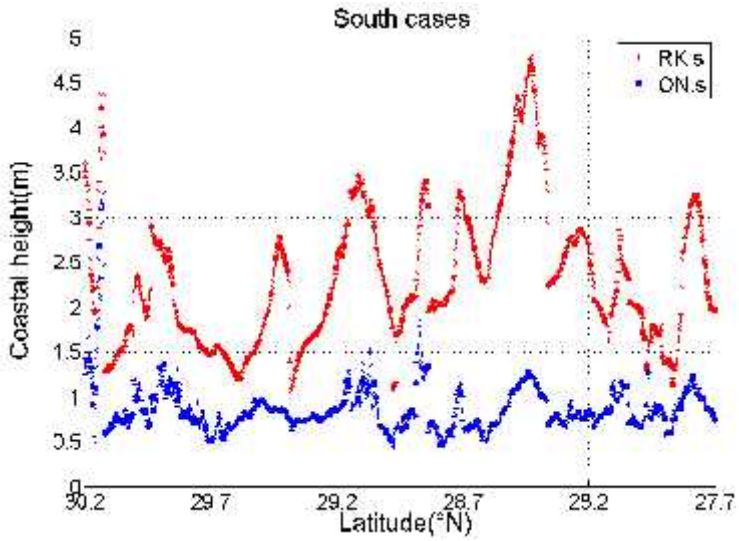


Figure 3.9 The maximum tsunami coastal heights comparison (South cases)

Consequently, same as the north cases, the tsunami in case RK.s has higher coastal heights than it in case ON.s in terms of the Chinese coast.

## 4. Inundation map of the worst scenario

Generally, tsunami generated in Ryukyu trench will cause more severe tsunami hazard to the Chinese coast than it generated in Okinawa trough. Moreover, if we take a close look at North cases, we will find that most of high coastal waves are around small islands or uninhabited areas. Therefore, the tsunami generated in south Ryukyu trench is selected as the worst tsunami scenario for the Chinese coast. The maximum coastal heights along Zhejiang province is about 5m, much higher than it showed in previous studies which is about 2-3m. So it is used to make inundation map for coastal cities.

### 4.1 Inundation map

At first, inundation map is made without consideration of tide effect. Among the Zhejiang coast, there are three major cities bearing tsunami risks in East China Sea: Zhoushan, Taizhou and Wenzhou. For the case RK.s, Zhoushan is fortunately protected from tsunami hazard by the islands located in front of it. Wenzhou is also protected by islands, but one of the islands, Dongtou district of Wenzhou with large population is highly

inundated. The only protection of Taizhou is Dachen island. However, both Taizhou and Dachen island cannot escape from the claws of tsunami inundation. The inundation maps are shown in Figure 4.1 a and b.

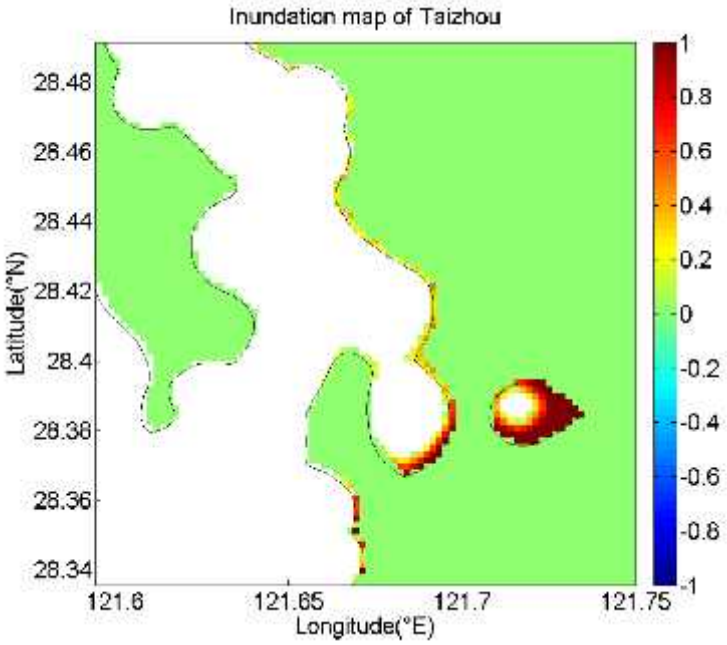


a) Inundation map of Taizhou

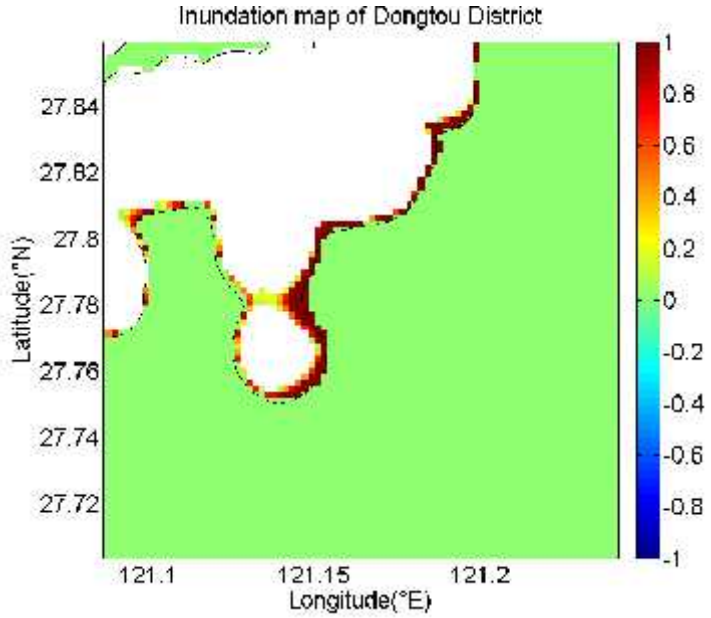


b) Inundation map of Dongtou District

Figure 4.1 Inundation map of the worst tsunami scenario

In addition, tidal difference along the Zhejiang coast is always above 4m (Cai et al. 2013). It is necessary to take tidal effect into account. Inundation map of Taizhou after 2m tide added is shown in Figure 4.2.

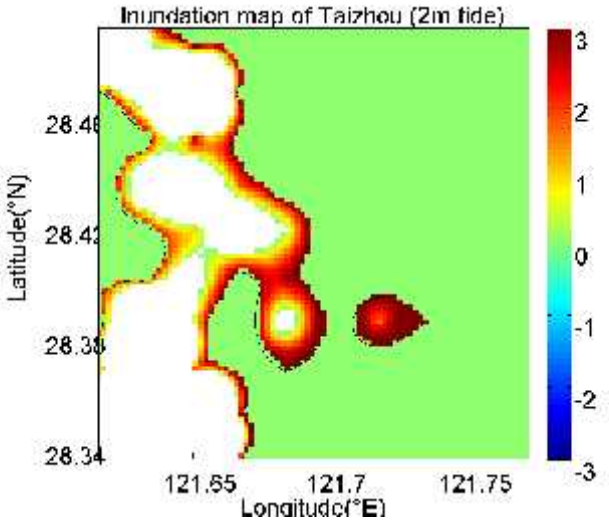


Figure 4.2 Inundation map of Taizhou (2m tide added)

The bathymetry and topography data used in this study is 1 arc-min resolution, even they are interpolated into about 200m in the third layer of nested grid, they differ from the actual situation due to the existence of small islands. Although Figure 7 shows inundation area increased largely after 2m tide added, actual inundated area could be less after high-resolution bathymetry and topography data are employed.

## 5. Conclusion

The conclusion of this study is summarized as follows:

1.In this study, we have conducted four hypothetical tsunami simulations. Tsunamis generated in Ryukyu trench are more threatening than that generated in a parallel position of Okinawa trough.

2. We have found a tsunami source (case RK.s) which can possibly be the worst tsunami scenario for the Chinese coast. The maximum coastal height along Zhejiang province is about 5m, much higher than that showed in previous studies which is about 2-3m.

3. The worst tsunami scenario (case RK.s) is used for tsunami inundation calculation. Taizhou, Dongtou district of Wenzhou, Dachen island are highly inundated. Their populations are over 1 million, 100 thousand, 1 thousand respectively. Without any protection like seawall, it will easily cause hundreds of life casualties and huge economic loss. The inundation distance is up to about 800m.

4. Inundation area will be largely increased if tide level is added into the calculation. But it may be exaggerated due to the coarse resolution of bathymetry and topography data used in this study.

## 6. Future study

More rigorous study about tsunami run-up should be carried out in the future study. In addition, incorporate high resolution of bathymetry and topography data into the numerical model will also be needed for a solid foundation for tsunami hazard mitigation plan of coastal cities.

## References

Wang Feng, Liu Changsen, Zhang Zhenquan (2005) Earthquake tsunami record in Chinese ancient books. Earthquake research in China. Vol.21 No.3 437-443. (in Chinese)

Chen Yong, Chen Qifu, Zhang Wei (2007) Tsunami disaster in China. Journal of natural disasters. Vol.16 No.2 1-5 (in Chinese)

Ren Yefei, Wen Ruizhi, Song Yuying (2014) Recent progress of tsunami hazard mitigation in China. Episodes Vol.37, No.4: 277-283

Tokutaro Hatori (1988) Tsunami magnitudes and source areas along the Ryukyu islands. Earthquake Vol.2 No.41 541-547 (in Japanese)

Wang Pinxian, Li Qianyu, Li Chunfeng (2014) Geology of the China Seas.

Li Xiaojun (2006) Special problems on evaluation of seismic safety for offshore engineering site. Technology for Earthquake Disaster Prevention Vol.1, No.2 (in Chinese)

Mao Xianzhong, Zhu Qian, Wei Yong (2015) Risk analysis of potential regional earthquake tsunami on the coast of Zhejiang Province. Haiyang Xuebao, Vol.37, No.3. (in Chinese)

Wen Yanlin, Zhao Wenzhou, Li Wei, Xue Yan, Yu Haiying (2014) Research on the potential tsunami hazard in East China Coast under rare earthquake occurred in Nankai Trough, Japan. Acta Seismologica Sinica, Vol.36, No.4. (in Chinese)

Wen Yanling, Liu Shuangqing, Zhu Ailan, Song zhiping, Li Chunfeng (2016) Numerical simulation of risk in the southeast coastal region of China owing to a rare earthquake-induced tsunami in the Ryukyu trench. China earthquake engineering journal, Vol.38, No.2. (in Chinese)

Lin Faling (2012) Numerical simulation of the effect of the “3.11” Japan earthquake tsunami and the hypothetical earthquake tsunami at South China Sea and the Ryukyu Islands on Fujian offshore area. Journal of Oceanography in Taiwan strait, Vol.31, No.4. (in Chinese)

Liu Shuangqing, Zhu Yuanqing, Liang Mingjian, Dong Feifei (2012) Impact of potential tsunami induced by Okinawa trough earthquakes on southeastern seaboard of China. Acta seismologica sinica. Vol.34, No.3 283-295. (in Chinese)

Liu Yingchun, Shi Yaolin, David A. Yuen, Erik O.D.Sevre, Yuan Xiaoru, Xing Linghui (2009) Comparison of linear and nonlinear shallow wave water equations applied to tsunami waves over the China Sea. Acta Geotechnica 4: 129-137

Zhiyuan Ren, Xi Zhao and Hua Liu (2015) Dispersion effects on tsunami propagation in South China Sea, Journal of Earthquake and Tsunami, Vol.9, No.5

Mei, C.C. (1989) The applied dynamics of ocean surface waves.

Shuto, N, et al (1986) A study of numerical techniques on the tsunami propagation and run-up, Sci.Tsunami Hazard 4, 111-124

P.L.-F.Liu, Y-S. Cho, M.J.Briggs, C.E. Synolakis, and U.Kanoglu. (1995) Run-up of solitary waves on a circular island. J.Fluid Mech, 302:259-285

X.Wang and P.L.-F.Liu. (2006) An analysis of 2004 sumatra earthquake fault plane mechanisms and indian ocean tsunami. J.Hydraulic Res., 44(2):147-154

M. Okada (1985) Surface deformation due to shear and tensile faults in a half-space. Bull.Seism.Soc.Am., 75(4):1135-1154

Utsu T (2001) Seismology, 3rd edn. Kyoritsu Shuppan Co Ltd, Tokyo (in Japanese)

Isamu Aida (1981) Numerical experiments of historical tsunamis generated off the coast of the Tokaido District. Bull.Earthq.Res.Inst, Vol.56, 367-390 (in Japanese)

Isamu Aida (1981) Numerical experiments of the tsunamis generated off the coast of the Nankaido District. Bull.Earthq.Res.Inst, Vol.56, 713-730 (in Japanese)

Harada and Satake (2014) Tsunami simulations in the Western Pacific Ocean and East China Sea from the Great Earthquakes along the Nankai-Suruga Trough. Tsunami Events and Lessons Learned: Environmental and Societal Significance, Chapter 6.

SatByul Kim, Tatsuhiko Saito, Eiichi Fukuyama and Tae-Seob Kang (2016) The Nankai Trough earthquake tsunamis in Korea: numerical studies of the 1707 Hoei earthquake and physics-based scenarios. Earth, Planets and Space. 68:64

Peter Bird (2003) An updated digital model of plate boundaries. Geochemistry Geophysics Geosystems, Vol.4, No.3.

Yufang Rong, David D.Jackson, Harold Magistrale and Chris Goldfinger (2014) Magnitude limits of subduction zone earthquakes. Bulletin of the Seismological Society of America, Vol.104, No.5.

Jingyi Lin, Jean Claude Sibuet, Shukun Hsu and Wennan Wu (2014) Could a Sumatra-like megathrust earthquake occur in the south Ryukyu subduction zone? Earth, Planets and Space 66:49

**Acknowledgements**

I am greatly appreciated my advisor Professor Akio Okayasu for he opens the door of coastal engineering to me and changes the way of my thinking which I see as the most valuable spiritual assets I gained during my study. Although I have a long way to improve, I am heartily grateful to him.

I would also like to thank gratefully to Professor Ikeya, Associate Professor Inazu in our Coastal Engineering & Environment Laboratory and Professor Tani in our university for their patience and fruitful help. This study would not come this far without their aids.

The numerical model COMCOT used in this study is provided by Professor Philip Liu and Dr. Xiaoming, Wang from Cornell University. Here, I also want to show my special thanks to them.

I also want to extend my thanks to my friends in the laboratory and school for their help in my life and study in Japan.

This research journey will be void without my family support. I am thankful to their motivation and anything else they have given.